Diseases of the nervous system associated with calcium channelopathies

Todorov, B.B.

ENHANCED GRANULE CELL OUTPUT AND IRREGULAR PURKINJE CELL FIRING IN GAIN-OF-FUNCTION *CACNA1A*^{S218L} MUTATION

Zhenyu Gao[1], Boyan Todorov[2], Curtis F. Barrett[2,3], Stijn van Dorp[4], Michel D. Ferrari[3], Arn M.J.M. van den Maagdenberg[2,3], Chris I. De Zeeuw[1,4], and Freek E. Hoebeek[1]*

[1]Department of Neuroscience, Erasmus MC, Rotterdam, The Netherlands; Departments of [2]Human Genetics, and [3]Neurology, Leiden University Medical Centre, Leiden, The Netherlands; [4]Netherlands Institute for Neuroscience, Royal Academy of Arts & Sciences (KNAW), Amsterdam, The Netherlands

Submitted

ABSTRACT

Mutations in the *CACNA1A* gene are associated with neurological disorders, such as ataxia, hemiplegic migraine, and epilepsy. These mutations can be categorized by their effects on Ca^{2+}-channel function as either loss- or gain-of-function mutations. While recent evidence demonstrates that loss-of-function mutations decrease the regularity of cerebellar Purkinje cell activity and thereby induce cerebellar ataxia, it is unknown how gain-of-function mutations induce ataxia. Using gain-of-function *Cacna1a*^{S218L} knockin mice, we show that both synaptic connectivity and transmission between granule cells and Purkinje cells are increased. Additionally, *Cacna1a*^{S218L} Purkinje cells show hyperexcitable action potentials and dendritic Ca^{2+}-spike firing, which deregulates their spontaneous firing pattern and can be counteracted by Ca^{2+}-dependent K^+-channel activators. Our findings illustrate the underlying mechanisms of ataxia with gain-of-function mutations, which are surprisingly similar to those seen in loss-of-function *Cacna1a* mutants. This commonality reveals the existence of a narrow window for optimal Ca^{2+}-homeostasis: sufficiently increased or decreased Ca^{2+}-influx induces ataxia.

INTRODUCTION

Since the entry of Ca^{2+}-ions via voltage-gated Ca^{2+}-channels (VGCCs) controls crucial processes in mammalian neurons, such as neurotransmitter release, synaptic plasticity, and membrane excitability, mutations that affect VGCC functioning are likely to have severe effects (as reviewed by *Catterall et al., 2008*). For instance, mutations in the *CACNA1A* gene, which encodes the α_{1A} subunit of $Ca_V2.1$ (P/Q-type) VGCCs, are associated with various neurological disorders, including ataxia, hemiplegic migraine, and epilepsy (*Vahedi et al., 1995*; *von Brederlow et al., 1995*; *Ophoff et al., 1996*; *Imbrici et al., 2005*).

Mutations in $Ca_V2.1$ channels can be divided into gain- and loss-of-function mutations, depending on whether the mutation increases or decreases channel function, respectively. Recent studies suggested a clear division in phenotypes induced by loss-of-function and gain-of-function mutations. Gain-of-function mutations in the *CACNA1A* gene are linked to familial hemiplegic migraine type 1 (FHM1) (*van den Maagdenberg et al., 2004*; *Tottene et al., 2005*; *Catterall et al., 2008*), whereas hereditary forms of ataxia induced by mutations in the *CACNA1A* gene, like episodic ataxia type 2 (*Ophoff et al., 1996*; *Zhuchenko et al., 1997*), are currently known as the result of loss-of-function mutations. Studies of natural mouse mutants bearing mutations in the orthologous mouse *Cacna1a* gene, such as *tottering*, *leaner*, and *rolling Nagoya* mice (*Fletcher et al., 1996*; *Mori et al., 2000*), revealed that loss-of-function mutations consistently induce altered connectivity and transmission at the parallel fiber-Purkinje cell (PF-PC) synapse, as well as irregular Purkinje cell activity (*Wakamori et al., 1998*; *Rhyu et al., 1999a*; *Matsushita et al., 2002*; *Hoebeek et al., 2005*; *Walter et al., 2006*). These aberrations have been shown to disturb the information processing in the cerebellar cortex (*Hoebeek et al., 2005*) and therefore are considered true hallmarks of cerebellar ataxia.

Although it is clear that inadequate Ca^{2+}-influx, as found in loss-of-function *Cacna1a* mutants, can induce both developmental and electrophysiological aberrations that eventually lead to ataxia, it remains to be elucidated why FHM1 patients with the gain-of-function S218L mutation in the *Cacna1a* gene are ataxic (*Kors et al., 2001*). In order to reveal the underlying mechanism of ataxia, we performed a detailed morphological and electrophysiological analysis of *Cacna1a*^{S218L} knockin mice (*van den Maagdenberg et al., 2010*). Our results show that both synaptic connectivity and transmission between granule cells and Purkinje cells are enhanced and that Purkinje cells show distinct signs of hyperexcitability, which together induce irregular Purkinje cell firing and can be counteracted by the activation of Ca^{2+}-dependent K^+-channels. Thus, our data reveal not only key cerebellar hallmarks of ataxia in the *Cacna1a*^{S218L} gain-of-function mouse model that resemble those in loss-of-function *Cacna1a* mutants, but also a striking similarity in the counteractive pathway.

EXPERIMENTAL PROCEDURES

Animals

Forty-two homozygous *Cacna1a*^{S218L} mice and 45 wild-type littermates (both genders) ranging from postnatal day (P) 5 to 3 months old were used in the experiments. Animals were maintained at 22 ± 2°C with 12hrs dark and light cycle and were provided with food and water *ad libitum*. All studies were performed in accordance with the guidelines of the respective universities and national legislation.

Immunohistochemistry

Four 2-month-old *Cacna1a*^{S218L} mice and four wild-type littermates were anaesthetized with Nembutal (50 mg/kg i.p.) and perfused transcardially with 50 ml phosphate-buffered saline (PBS) (pH 7.4) containing 4% paraformaldehyde. The cerebellum was carefully removed and post-fixed in fresh fixative for 2hrs at room temperature. Sixty-µm thick parasagittal sections were sliced with a cryotome (*Leica, Wetzlar, Germany*), collected in 0.1 M PBS and rinsed in 50 mM PBS. Free-floating slices were blocked with 10% normal horse serum (NHS) and 0.5% Triton-X100 for 1h and incubated with rabbit anti-calbindin D-28K antibody (1:10,000, *Sigma-Aldrich, Zwijndrecht, Netherlands*), diluted in PBS with 2% NHS and 0.5% Triton-X100 for 72hrs. Subsequently, slices were incubated with biotinylated goat-anti-rabbit secondary antibody (1:200; *Vector Laboratories, Burlingame, CA*) for 1.5hrs and followed by a 1.5h incubation with avidin-biotinylated horseradish peroxidase complex (ABC-HRP, *Vector Laboratories*). Sections were rinsed in 0.1 M phosphate buffer and visualized with 0.05% 3,3-diaminobenzidine tetrahydrochloride. After rinsing in 0.1 M PBS, the slices were mounted and counterstained using Nissl staining.

Electron microscopy

Four 2-month-old *Cacna1a*^{S218L} mice and four wild-type littermates were anaesthetized with Nembutal (50 mg/kg i.p.) and perfused transcardially with 50 ml 0.12 M phosphate buffer (pH 7.4) containing 4% paraformaldehyde and 0.2% glutaraldehyde. Next, cerebella were cut into 80-100 µm sections using a vibratome (*Technical Products International, St. Louis, MO*) and collected in 0.12 M phosphate buffer. Sections were post-fixed in 1% osmium tetroxide, stained with 1% uranyl acetate, dehydrated, and embedded in Araldite (*Durcupan ACM, Fluka, Germany*). Ultrathin (50-70 nm) sections were then cut using an ultramicrotome (*Leica*), mounted on Formvar-coated copper grids, contrasted with 2% uranyl acetate and 1% lead citrate (*Fluka*), and analyzed using a CM100 electron microscope (*Philips, Eindhoven, The Netherlands*). Electron micrographs were collected with a CCD-camera (*Megaview II, Olympus Soft Imaging System, Munster, Germany*) and analyzed with AnalySIS (*Olympus Soft Imaging System*) and MetaVue (*Universal Imaging Corp., San Francisco, CA*) image processing software. To estimate the average numbers of Purkinje cell spines and parallel fiber

varicosities, 25 images of the most distal 1/3 of the molecular layer were collected per animal at 13,500×. PF-PC synapses were recognized as asymmetrical contacts with loosely clustered spherical synaptic vesicles in PF varicosities and clear postsynaptic density structures in Purkinje cell spines. CF-PC synapses were identified by their more proximal location and high number of tightly compacted vesicles. The morphology of parallel fiber varicosities and Purkinje cell spines was analyzed at 19,000×. To verify the percentage of parallel fiber varicosities that contact multiple Purkinje cell spines, 1000 synaptic contacts per genotype were quantified. To quantify the dimensions of the PF varicosity and dendritic spines > 50 structures per animal were used. The Purkinje cell spine length was calculated by measuring the distance between the tip of the spine head and the base of the spine neck. Electron micrograph analysis was performed by averaging per animal and then by genotype. Data are represented as mean ± S.E.M.

Slice preparation for electrophysiology

Thirty-four *Cacna1a*^{S218L} mutants and 37 wild-type littermates of various ages (*see below*) were decapitated under isoflurane anesthesia. Subsequently, the cerebellum was removed and transferred into ice-cold slicing medium that contains (in mM): 240 sucrose, 5 KCl, 1.25 Na_2HPO_4, 2 $MgSO_4$, 1 $CaCl_2$, 26 $NaHCO_3$ and 10 D-glucose, bubbled with 95% O_2 and 5% CO_2. Parasagittal slices (200 or 250 µm thick) of the cerebellar vermis were cut using a vibratome (VT1000S, *Leica*) and kept in ACSF containing (in mM): 124 NaCl, 5 KCl, 1.25 Na_2HPO_4, 2 $MgSO_4$, 2 $CaCl_2$, 26 $NaHCO_3$ and 20 D-glucose, bubbled with 95% O_2 and 5% CO_2 for > 1h at 34 °C before the experiments started. All chemicals were obtained from *Sigma-Aldrich*.

Whole-cell electrophysiology

Experiments were performed with a constant flow of oxygenated ACSF (2.5-3.0 ml/min). Purkinje cells were visualized using an upright microscope (Axioskop 2 FS plus, *Carl Zeiss, Jena, Germany*) equipped with a 40× water immersion objective. Patch-clamp recordings were performed using an EPC-10 amplifier (*HEKA Electronics, Lambrecht, Germany*). Voltage clamp recordings were performed at room temperature whereas current clamp and loose cell-attached recordings were performed at 35 ± 1°C.

Parallel fiber response

Four 2- to 3-month-old *Cacna1a*^{S218L} mutants and five wild-type littermates were used to record Purkinje cell responses to PF stimulation. The resistances of borosilicate patch pipettes ranged from 2.8 to 3.5 MΩ when filled with intracellular solution containing (in mM): 70 Cs-Methalsulfonate, 80 CsCl, 2 $MgCl_2$, 1 EGTA, 10 HEPES, 4 Na_2ATP and 0.4 Na_3GTP (pH 7.3). Membrane potentials were clamped at -70 mV with holding currents ranging from -100 to -200 pA. A voltage step of -10 mV was applied following each stimulus to monitor series and input resistances. Cells were discarded if the input resistance was < 150 MΩ or when series and/or input resistance shifted

more than 15% during the recording. To evoke PF-mediated excitatory postsynaptic currents (PF-EPSCs), patch pipettes filled with ACSF were placed in the most distal 1/3 of the molecular layer adjacent to the patched Purkinje cells at the same distance and orientation. To assess the stimulus intensity-EPSC output (input-output) ratio consistently, only Purkinje cells with similar dendritic arborization (based on the width of molecular layer) were selected. To elicit paired-pulse facilitation, two consecutive stimuli were given with 25-500 ms inter-stimulus intervals. PF-EPSC kinetics were characterized by calculating the 10-90% rise time and τ_{decay} using a single exponential fit (*IGOR pro, Wavemetrics, Portland, OR*) of averaged (4-6 subsequent) PF-EPSCs recorded in response to stimuli of 10 μA.

Estimation of VGCC subtypes that contribute to neurotransmitter release at PF-PC synapse

Four 2- to 3-month-old *Cacna1a*^{S218L} mutants and four wild-type littermates were used to estimate the EPSC fractions controlled by different VGCC subtypes. N-type blocker ω-Conotoxin GVIA (ω-CgTx) and P/Q-type blocker ω-Agatoxin-IVA (ω-Aga-IVA) were bath-applied after stable baseline EPSCs were obtained. Reductions of relative EPSCs were taken as functional indications after each blocker was applied. Both ω-CgTx and ω-Aga-IVA were obtained from *Peptide Institute* (*Osaka, Japan*). Stock solutions were prepared in ACSF in the presence of 1 mg/ml cytochrome C to minimize nonspecific binding. Stock solutions (0.1 mM concentrations) were stored at -20°C and used within two weeks. ω-CgTx and ω-Aga-IVA stocks were diluted in ACSF supplemented with 0.1 mg/ml cytochrome C, yielding final concentrations of 3 μM ω-CgTx and 0.2 μM ω-Aga-IVA.

Climbing fiber response

To minimize space-clamp error, young animals (6 *Cacna1a*^{S218L} mutants and 6 wild-type littermates) ranging from P16 to P21 were used (*Llano et al., 1991*). Additionally, to avoid Na^+-spikes, we included 5 mM QX-314 in the Cs^+-based intracellular solution. To standardize the driving force, we continuously clamped the membrane potential at -20 mV from the reversal potential. Only cells with a low initial series resistance of 8-12 MΩ and a series resistance that was compensated for > 70% were included in the study. Reversal potentials were measured before and after experiments and cells were excluded if the reversal potential shifted > 3 mV. Stimulation electrodes were placed in the granule cell layer surrounding the Purkinje cell somata. We checked for Purkinje cells innervated by multiple climbing fibers by gradually increasing the stimulus intensity while recording CF-EPSCs. Purkinje cells that responded with a stepwise increase of CF-EPSC amplitude were considered to be innervated by multiple climbing fibers (*Hansel et al., 2006*) and were excluded from further analysis. Paired-pulse depression was measured using two stimulation pulses with inter-stimulus intervals ranging from 50 to 800 ms. CF-EPSC kinetics where characterized by calculating the 10-90% rise time and the single-exponential τ_{decay} of averaged (4-6 consecutive) CF-EPSCs (*IGOR pro, Wavemetrics, Inc., Portland, OR*).

Ca^{2+}-current in Purkinje cells

Whole-cell Ca^{2+}-currents were recorded in Purkinje cells from four *Cacna1a*^{S218L} mutant and four wild-type P5 animals using an intracellular solution containing (in mM) 100 Cs-Methalsulfonate, 2 $MgCl_2$, 20 TEA, 10 EGTA, 5 QX-314, 10 HEPES, 10 Na-Phosphocreatine, 4 Na_2ATP, and 0.4 Na_3GTP (pH 7.3). Additionally, 1 µM TTX and 2.5 mM 4-AP were added extracellularly. The series resistance was compensated for > 70% and leak and capacitive currents were subtracted by the -P/4 method. Cells were discarded when the holding current at -80 mV exceeded -200 pA. Ca^{2+} currents were obtained by 50 ms depolarizing pulses to various membrane potentials ranging between -80 and +40 mV at 5 mV increments. Current-voltage (I-V) curves were obtained only from cells with a voltage error of < 5 mV and without any signs of inadequate voltage-clamp as measured by notch-like current discontinuities and slow components in the decay of capacitative currents (in response to hyperpolarizing pulses). The current density was calculated by dividing the current amplitude by the cells capacitance. We considered currents > 3 SD from the average holding current to be detectable currents.

Purkinje cell spontaneous activity and current clamp recording

The Purkinje cell spiking activity was recorded in loose cell-attached configuration with patch pipettes (diameter 2-3 µm) filled with ACSF. Eight 2- to 3-month-old *Cacna1a*^{S218L} mutants and 10 wild-type littermates were used in this experiment. Spontaneous activity was observed as fast current deflections of -100 to -200 pA. Analysis of the regularity of spiking and the frequency was performed with MATLAB (*Mathworks*) and Excel (*Microsoft*) using the first 5,000 spikes recorded from each cell. The regularity of firing was calculated using the second coefficient of variance (CV2), to quantify the instantaneous regularity of firing ($CV2 = 2|ISI_{n+1}-ISI_n|/(ISI_{n+1}+ISI_n)$) (*Holt et al., 1996*). Autocorrelograms of ISIs were generated using a 1 ms bin width as previously described (*Hoebeek et al., 2005*) using custom-made MATLAB scripts.

For current clamp experiments, an intracellular solution containing (in mM) 120 K-gluconate, 9 KCl, 10 KOH, 3.48 $MgCl_2$, 4 NaCl, 10 HEPES, 4 Na_2ATP, 0.4 Na_3GTP and 17.5 sucrose (pH 7.25) was used. Purkinje cells from eight 2- to 3-month-old *Cacna1a*^{S218L} mutant and eight wild-type animals were held at -65 to -70 mV using -400 to -500 pA current injection to avoid spontaneous spiking activity. To study the effects of PF input on Purkinje cell spiking patterns, holding current injections were cancelled to allow spontaneous firing. For current injection experiments, after obtaining stable holding potentials, spiking patterns were elicited by injection of depolarizing currents ranging from 100 to 1000 pA (relative to the holding current).

Computational modeling

Mechanisms of dendritic calcium spikes were simulated in a single-compartment model of an isolated piece of Purkinje cell dendrite, using the NEURON environment (For details see *supplemental experimental procedures*).

Statistics

Statistical comparison between *Cacna1a*^{S218L} mutants and wild-type littermates was performed using paired or unpaired two-tailed Student's *t*-test, with $p < 0.05$ defining a significant difference. Summarized data are represented as mean ± S.E.M.

RESULTS

Normal cerebellar structure but increased connectivity at *Cacna1a*^{S218L} PF-PC synapse

Given the widespread and dense expression of the *Cacna1a* gene in the rodent cerebellum (*Fletcher et al., 1996*; *Kulik et al., 2004*), we first quantified to what extent the gross morphology of the cerebellum is affected by the S218L mutation. Parasagittal slices taken from 2-month-old *Cacna1a*^{S218L} mice showed a normal cerebellar structure with no change in the foliation or organization of molecular, Purkinje cell, and granular layers (*Fig. 1A-D*). Also neither the estimated volume of the cerebellum nor the numbers of Purkinje cells of *Cacna1a*^{S218L} mutants was significantly different from those in wild-type mice (*Supplementary table 1*). Still, we can not rule out that the S218L mutation affects synaptic morphology, as ultrastructural aberrations of PF-PC synapses have been a consistent finding in loss-of-function *Cacna1a* mutants (*Rhyu et al., 1999a*). Therefore, we performed a detailed morphological study of the PF-PC synapse using electron microscopy and found that in both wild-type (c.f. *Fig. 1E*) and *Cacna1a*^{S218L} (c.f. *Fig. 1F*) tissue, PF-PC synapses appeared as asymmetrical contacts with loosely clustered spherical synaptic vesicles in PF varicosities and clear postsynaptic density structures in Purkinje cell spines. Both the density and dimensions of the PF varicosities and Purkinje cell spines in *Cacna1a*^{S218L} mutants were not significantly different from those in wild-type animals (*Supplementary table 1*). However, single PF varicosities contacted multiple Purkinje cell spines significantly more frequently in *Cacna1a*^{S218L} mutants than in wild-type mice ($p < 0.001$) (*Fig. 1G, H*). These results show that although there are no significant differences in the gross morphology of the cerebellar cortex of *Cacna1a*^{S218L} mutants, an increased number of their PF varicosities contact multiple Purkinje cell spines.

Increased synaptic transmission at *Cacna1a*^{S218L} PF-PC synapse

Given the increased synaptic connectivity between PFs and Purkinje cell spines, we measured the synaptic transmission at the PF-PC synapse by recording EPSCs in Purkinje cells in response to PF stimulation at geometrically determined locations in the molecular layer (c.f. *Experimental Procedures*). Systematically increasing the stimulus intensity yielded essentially linear input-output curves for both *Cacna1a*^{S218L} and wild-type synapses; however, with increasing stimulus intensity (> 8 μA) EPSCs were progressively larger in *Cacna1a*^{S218L} than in wild-type Purkinje cells (all $p < 0.05$) (*Fig. 2A*). In fact, at the maximum stimulus intensity tested (20 μA), the PF-EPSCs

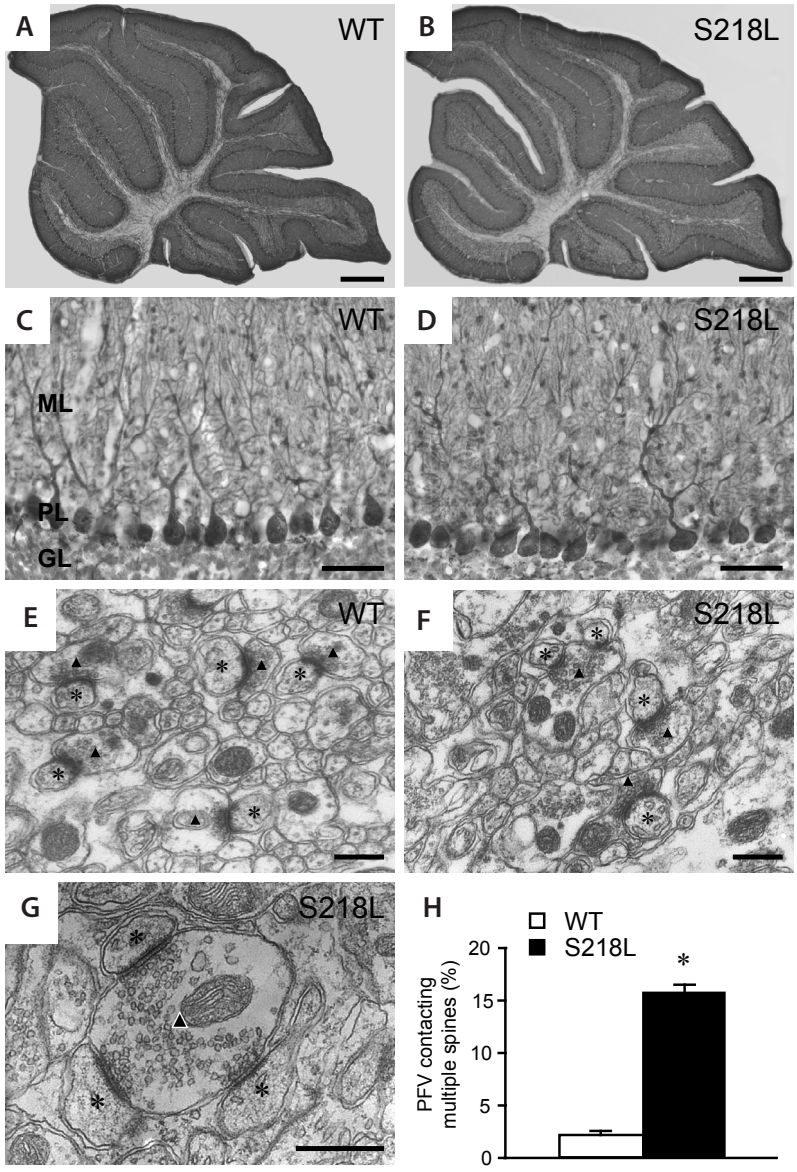

Figure 1. No change in gross cerebellar structure, but increased connectivity at PF-PC synapse in *Cacna1a*^{S218L} mice. (A, B) Overview of anti-calbindin D-28k and Nissl-stained mid-sagittal cerebellar sections from wild-type and *Cacna1a*^{S218L} animals (scale bars: 500 µm). **(C, D)** High magnification of anti-calbindin, and Nissl-stained Purkinje cells in wild-type and *Cacna1a*^{S218L} cerebellum (scale bars: 50 µm), ML - molecular laye; PL - Purkinje cell layer; GL - granule cell layer. **(E, F)** Electron micrographs of distal PF-PC synapses. Triangles indicate the parallel fiber varicosity, asterisks indicate Purkinje cell spines (scale bars: 0.3 µm). **(G)** Multiple synaptic contacts between a single parallel fiber varicosity and three Purkinje cell dendritic spines (scale bar: 0.3 µm). **(H)** Percentages of parallel fiber varicosities that contact multiple Purkinje cell spines in wild-type mice (N = 3) and *Cacna1a*^{S218L} mutants (N = 3). Asterisks indicate significant difference (indicated in the results section). See also *Supplementary table 1*.

in *Cacna1a*^{S218L} mutants were ~30% larger than in wild-type, whereas the kinetics of the PF-EPSCs showed no significant differences between *Cacna1a*^{S218L} and wild-type ($p = 0.2$ for 10-90% rise time value and $p = 0.3$ for decay time constant (τ_{decay})) (*Supplementary fig. 1A*). These data indicate that the efficacy of synaptic transmission between granule cells and Purkinje cells in *Cacna1a*^{S218L} mutants is enhanced.

To investigate whether the increased synaptic transmission in *Cacna1a*^{S218L} mutants is solely due to the increased synaptic connectivity between granule cells and Purkinje cells, we separately studied the presynaptic component of the PF-PC synaptic transmission. First, we recorded the paired-pulse ratio between two successive PF-EPSCs, which is a facilitation of the second PF-EPSC and reflects the increased efficacy of vesicle release due to residual free Ca^{2+}-ions in the PF terminal. At inter-stimulus intervals of 25-100 ms the paired-pulse facilitation in *Cacna1a*^{S218L} was significantly smaller than in wild-type mice (all $p < 0.001$) (*Fig. 2B*). Second, we applied channel-specific Ca^{2+}-channel blockers to study the effects of the S218L mutation on neurotransmitter release mediated by $Ca_V2.2$ (N-type) and $Ca_V2.1$ (P/Q-type) VGCCs, which together mediate the bulk of neurotransmitter release from PFs. The contribution of N-type channels was measured by bath application of the N-type specific blocker ω-Conotoxin GVIA (ω-CgTx). We found that N-type channels have a smaller contribution to EPSC amplitude in *Cacna1a*^{S218L} mutants ($p = 0.004$) (*Fig. 2C*). Subsequent bath-application of the P/Q-type specific blocker ω-Agatoxin IVA (ω-Aga-IVA) further reduced the PF-EPSC amplitude in both wild-type mice and *Cacna1a*^{S218L} mutants to equal residual currents ($p = 0.8$). The residual currents were similar to when ω-Aga-IVA was applied without ω-CgTx in the bath ($p= 0.7$). Thus, although the effect of blocking P/Q-type-mediated presynaptic Ca^{2+}-influx on PF-PC synaptic transmission is not increased in *Cacna1a*^{S218L} mutants, we observed a possibly compensatory decrease in the percentage of N-type-mediated neurotransmitter release. Together these data indicate that the S218L mutation enhances the release of neurotransmitter from PFs, which along with the increased synaptic connectivity is likely to enhance the input that Purkinje cells receive from granule cells.

No increase in synaptic transmission at *Cacna1a*^{S218L} climbing fiber–Purkinje cell synapse

Since $Ca_V2.1$ VGCCs also mediate the transmission at the climbing fiber–Purkinje cell (CF-PC) synapse (*Regehr and Mintz, 1994*), we compared the Purkinje cell response to CF activation in *Cacna1a*^{S218L} mutants and found typical all-or-none responses with amplitudes and rise time values similar to those in wild-type littermates ($p > 0.2$), but a faster τ_{decay} ($p = 0.02$) (*Fig. 2D & Supplementary fig. 1B*). In order to clarify whether the S218L mutation altered the release probability at the CF synapse, we compared the response to double CF stimulations with inter-stimulus intervals ranging from 50 to 800ms. Such stimuli elicited similar paired-pulse ratios of CF-EPSCs in both *Cacna1a*^{S218L} mutants and wild-type littermates (all $p > 0.2$) (*Fig. 2E*), which indicated that, overall, the CF input to Purkinje cells is preserved in *Cacna1a*^{S218L} mutant mice.

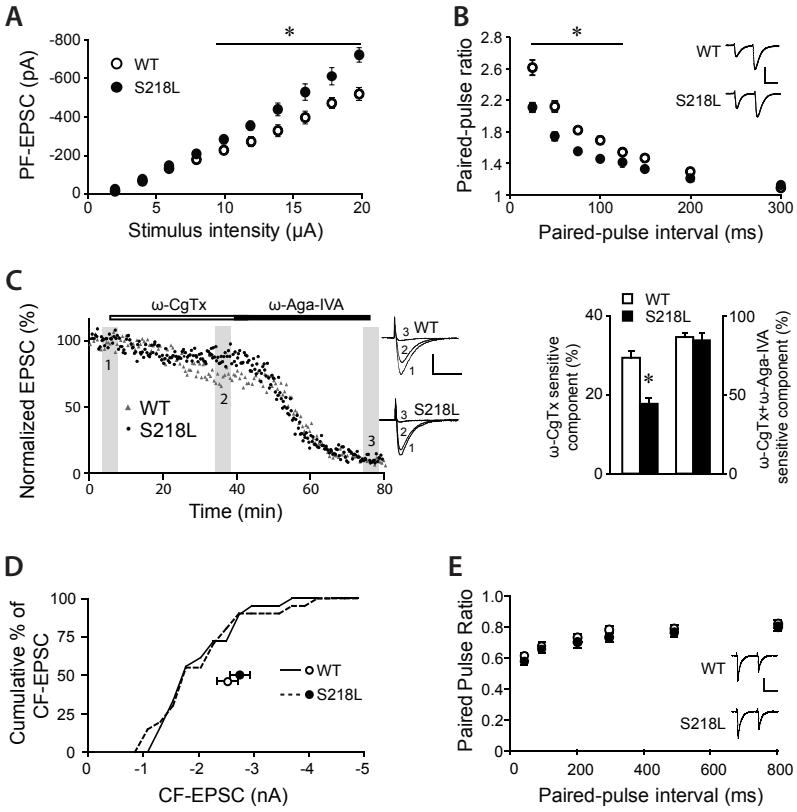

Figure 2. Increased synaptic transmission at PF-PC, but not CF-PC synapses. (A) Mean PF-EPSC amplitudes of wild-type (open circles, n = 8) and *Cacna1a*^{S218L} (solid circles, n = 10) Purkinje cells in response to increasing stimulus intensities. **(B)** Paired-pulse ratios (second EPSC/first EPSC) of PF-EPSCs with various paired stimulation intervals (25-300 ms) from wild-type (open circles, n = 8) and *Cacna1a*^{S218L} (solid circles, n = 8) Purkinje cells. Insets show representative paired PF-EPSCs with 50 ms inter-stimulus interval (scale bar: vertical 300 pA, horizontal 30 ms). **(C)** Left: Representative examples of the time course of PF-EPSC amplitudes of WT (grey triangle) and *Cacna1a*^{S218L} (black dots) Purkinje cells during the subsequent application of 3 μM ω-Conotoxin-GVIA (ω-CgTx) and 0.2 μM ω-Agatoxin-IVA (ω-Aga-IVA). The PF-EPSC amplitudes before toxin application were normalized to 100%. Insets represent example EPSC traces taken from indicated time points (scale bars: vertical 200 pA, horizontal 20 ms). Right: Summarized toxin-sensitive PF-EPSC components. **(D)** Dots indicate mean CF-EPSC amplitudes collected from wild-type (n = 21) and *Cacna1a*^{S218L} (n = 20) Purkinje cells. Lines indicate cumulative charts of CF-EPSC amplitude distributions of WT (continuous line) and *Cacna1a*^{S218L} (dashed line) Purkinje cells. **(E)** Paired-pulse ratios (second EPSC / first EPSC) of CF-EPSC with various stimulation intervals (50 - 800 ms) from wild-type (n = 23) and *Cacna1a*^{S218L} (n = 21) Purkinje cells. Insets show single CF-EPSC traces evoked by double CF stimulations with 50 ms inter-stimulus interval from wild-type and *Cacna1a*^{S218L} Purkinje cells (scale bars: vertical 1 nA, horizontal 20 ms). Asterisk indicates significant difference. See also *Supplementary figure 1*.

Altered Ca^{2+}-influx in *Cacna1a*^{S218L} Purkinje cells

Besides the altered synaptic inputs, *Cacna1a*^{S218L} Purkinje cells are likely to be affected intrinsically as 90% of their high-voltage activated Ca^{2+}-influx is mediated by P/Q-type channels (*Mintz et al., 1992*; *Wakamori et al., 1998*) and, moreover, cerebellar *Cacna1a*^{S218L} granule cells show a clear negative shift in their $Ca_V2.1$-channel activation curve (*Tottene et al., 2005*; *van den Maagdenberg et al., 2010*). In order to clarify to what extent $Ca_V2.1$-mediated Ca^{2+}-influx in Purkinje cells is changed by the S218L mutation, we recorded whole cell Ca^{2+} density. Wild-type Purkinje cells showed inward Ca^{2+} currents in response to depolarizing voltage steps from -40 ± 2 mV and peaked (-15.1 ± 1.3 pA/pF) at -10 mV (*Fig. 3A*). In contrast, *Cacna1a*^{S218L} mutant $Ca_V2.1$ channels in Purkinje cells activated at a more negative membrane potential of -48 ± 2 mV ($p < 0.002$ compared to wild-type) and peaked (-17.0 ± 1.5 pA/pF) at -25 mV. To quantify the effect of the mutation on voltage-dependent activation, we determined the normalized whole-cell conductance at each voltage and fit the data to a Boltzmann function, revealing a significant negative shift in $V_{1/2}$ of the *Cacna1a*^{S218L} neurons relative to wild-type neurons (-33.4 ± 1.1 mV vs. -21.6 ± 0.3 mV; $p < 0.001$) (*Fig. 3B*). The potency of this shift can be appreciated by considering the larger current density in *Cacna1a*^{S218L} neurons upon relatively mild depolarization (e.g., at –30 mV, at which currents through *Cacna1a*^{S218L} channels are 4 times greater

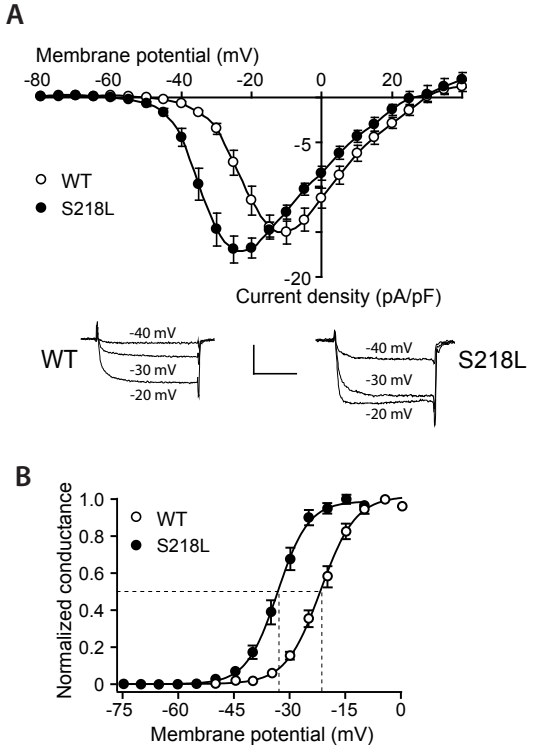

Figure 3. Negative shift of voltage-current relationships of whole cell Ca^{2+}-currents in *Cacna1a*^{S218L} Purkinje cells. **(A)** Voltage-current relationship of Ca^{2+}-current in wild-type (n = 14) and *Cacna1a*^{S218L} (n = 13) Purkinje cells. Mean current densities were plotted against depolarizing voltages. Insets show representative traces of Ca^{2+} currents in wild-type and *Cacna1a*^{S218L} Purkinje cells evoked by 50 ms depolarizing pulses to -40, -30, and -20 mV (holding potential = -80 mV; scale bars: vertical 10 pA/pF, horizontal 20 ms). **(B)** Normalized Ca^{2+}-conductance at different depolarizing voltages in wild-type (n = 14) and *Cacna1a*^{S218L} (n = 13) Purkinje cells. Solid curves indicate Boltzmann fits; dash lines indicate corresponding voltages of half-maximum conductance (p values are indicated in the Results section).

than though wild-type ones). Together these findings indicate that P/Q-type VGCCs in *Cacna1a*^{S218L} Purkinje cells respond more readily and robustly to changes in the membrane potential.

Irregular spontaneous spiking patterns in *Cacna1a*^{S218L} Purkinje cells

The increased granule cell input to Purkinje cells together with the negative shift in the activation curve of $Ca_V2.1$-channels in *Cacna1a*^{S218L} mutants predict that Purkinje cell activity is severely affected. In order to test this hypothesis optimally, we would have to record the Purkinje cell activity in awake, behaving animals. This, however, proved technically impossible in *Cacna1a*^{S218L} mutants due to the increased susceptibility to seizures and the increased death rate following even mild head trauma (see also *van den Maagdenberg et al., 2010*) inflicted by the necessary surgical preparations and restraining (*Hoebeek et al., 2005*). Therefore, we recorded activity patterns of Purkinje

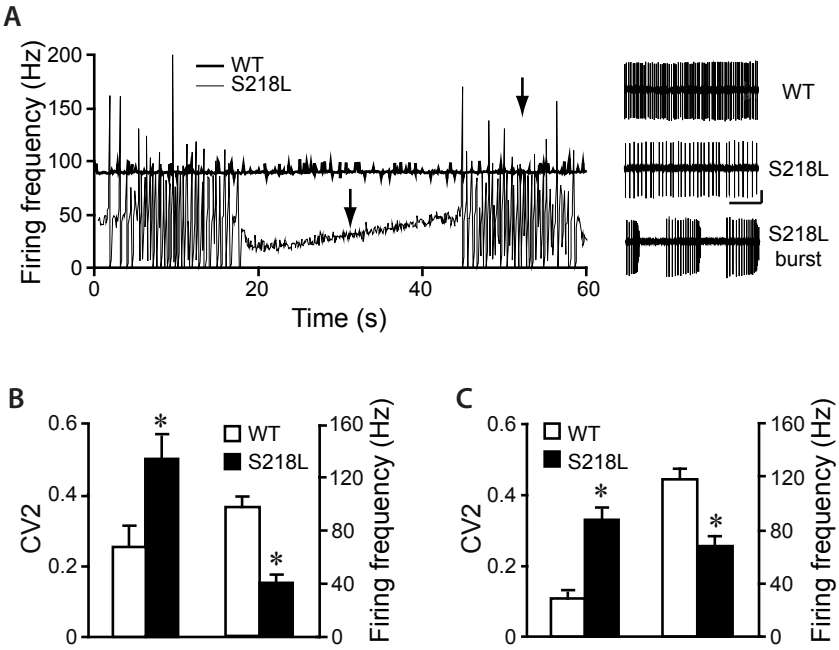

Figure 4. Irregular spontaneous activity of *Cacna1a*^{S218L} Purkinje cells. (A) Moving averages (bin width 100 ms) of 60 s of spontaneous firing frequency in wild-type (bold line) and *Cacna1a*^{S218L} (thin line) Purkinje cells. Left arrow indicates the time point of representative traces of continuous firing pattern in wild-type and *Cacna1a*^{S218L} shown in the top and middle insets and right arrow indicates *Cacna1a*^{S218L} burst pattern shown in the lower inset (scale bar: vertical 50 pA; horizontal 200 ms). **(B)** Mean second coefficient of variance (CV2) and firing frequency of spontaneous Purkinje cell activities from wild-type (n = 21) and *Cacna1a*^{S218L} (n = 26). **(C)** Similar to (B), but now representing pacemaking activity recorded from wild-type (n = 15) and *Cacna1a*^{S218L} (n = 15) Purkinje cells in the presence of blockers of all synaptic inputs (25 μM NBQX, 10 μM AP-V, and 10 μM Picrotoxin). Asterisks indicate significant differences (p values are indicated in the Results section). See also *Supplementary figure 2*.

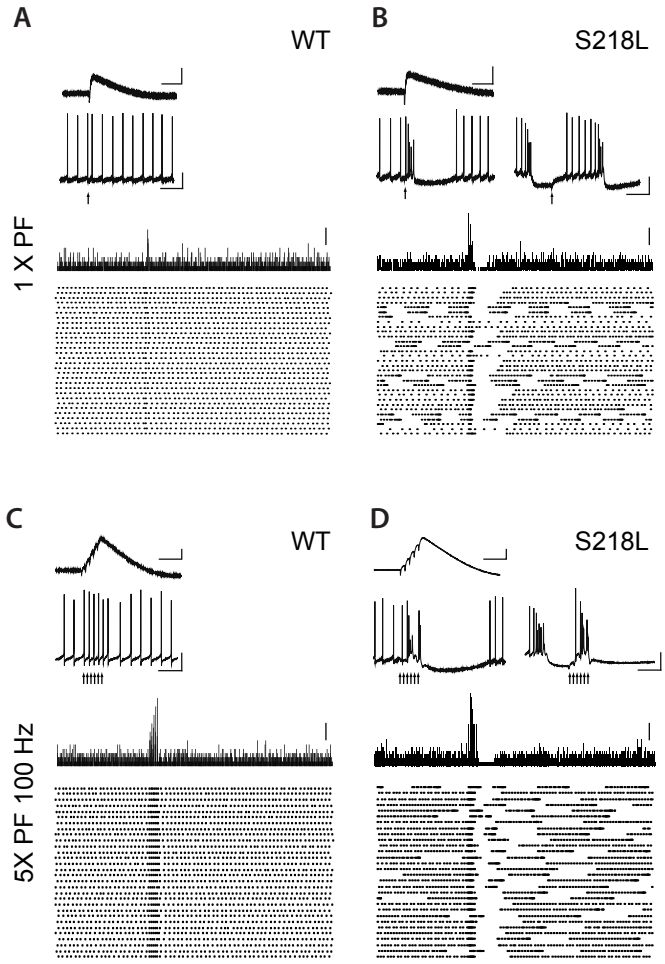

Figure 5. Modest PF stimulation induces Ca^{2+}-spikes in *Cacna1a*^{S218L} Purkinje cells. (A) (Top) Representative traces of 2 mV PF-EPSP (top inset, scale bars: vertical 2 mV, horizontal 50 ms) and typical Purkinje cell spiking pattern in response to PF stimuli (bottom inset, scale bars: vertical 20 mV, horizontal 50 ms). Vertical arrow indicates time of stimulation. (Bottom) Histogram of spike counts and accompanying raster plot of 30 repeats in response to single PF stimulation (scale bar: 4 spike counts). **(B)** Similar to (A) for a typical *Cacna1a*^{S218L} Purkinje cell that showed intermittent continuous and bursting episodes. Bottom insets show representative responses to single PF stimulations while the neuron fired continuously (left) or burst-like (right) prior to the stimulus. Note that when the *Cacna1a*^{S218L} Purkinje cell fired continuously, the single PF-EPSP induced a burst. In contrast, when the Purkinje cell fired bursts the single PF stimulation depolarized the membrane potential to reset the burst-pause-burst cycle. **(C, D)** similar to (A, B) but now for a 100Hz train of 5 PF stimuli. **(C)** Wild-type Purkinje cells respond with an action potential to each individual PF stimulus in the train (bottom inset). Scale bars: for PF-EPSP, vertical 4 mV, horizontal 50 ms; for action potential, vertical 20 mV, horizontal 50 ms; for histogram: 4 spike counts. **(D)** *Cacna1a*^{S218L} Purkinje cells always responded with a burst to the PF train stimulus, regardless of the pre-stimulus firing pattern.

cells in acutely prepared cerebellar slices using loose cell-attached recordings at physiologically relevant temperatures (35 ± 1°C). Under these conditions, the Purkinje cell spiking activity appeared as continuous regular spiking in 20 out of 21 recorded wild-type cells, but in only 2 out of 25 recorded *Cacna1a*^{S218L} Purkinje cells; the majority of the *Cacna1a*^{S218L} Purkinje cells showed an intermittent firing pattern (*Fig. 4A*) where periods of continuous firing (28 ± 5s) were interrupted by bursting activity (33 ± 10s). As a result, both the regularity and the average firing frequency of *Cacna1a*^{S218L} Purkinje cell activity were significantly different, in that the second coefficient of variance (CV2) (see *Experimental procedures*) was higher and the average firing frequency was lower ($p = 0.003$ and $p < 0.001$, respectively) (*Fig. 4B & Supplementary fig. 2A*). In order to test whether this irregular spontaneous firing pattern was caused by disturbed intrinsic pacemaking activity, we repeated the loose-cell attached recordings in the presence of blockers for all synaptic transmissions. These recordings revealed that indeed *Cacna1a*^{S218L} Purkinje cells show a severely disturbed intrinsic pacemaking activity (*Fig. 4C & Supplementary fig. 2B*), which was similar to the spontaneous Purkinje cell firing (all $p > 0.2$).

Parallel fiber activity elicits burst-like activity in *Cacna1a*^{S218L} Purkinje cells

Granting the irregular pacemaking activity in *Cacna1a*^{S218L} Purkinje cells, we next studied the effects of PF input on spontaneous Purkinje cell activity. To do so, we first adjusted the PF stimulation to elicit physiologically relevant PF-EPSPs of 2 mV (see *Experimental Procedures*) in both groups, by which we canceled any influence of the differences in the PF input strength (see *Fig 2.*). Single pulse stimulations resulted in well-timed action potential firing in the spontaneous firing of all 12 wild-type Purkinje cells, but elicited a burst and subsequent pause in 12 out of 13 *Cacna1a*^{S218L} Purkinje cells (*Fig. 5A, B*). In *Cacna1a*^{S218L} Purkinje cells that were firing bursts, the stimulus seemed to reset the burst-like firing state (*Fig. 5B*). Moreover, this difference in response pattern to PF stimuli between wild type and *Cacna1a*^{S218L} Purkinje cells persisted when we applied a stimulus train at a physiologically relevant frequency (100Hz) (*Jorntell & Ekerot, 2006*) (*Fig. 5C, D*); all wild-type cells (n = 8) responded with a short period of higher firing frequency whereas the train stimuli in the *Cacna1a*^{S218L} Purkinje cells (n = 10) consistently induced bursts, regardless of the preceding activity patterns. Thus, excitatory synaptic input from granule cells elicits burst-like firing in *Cacna1a*^{S218L} Purkinje cells, which together with the concurrent irregular pacemaking activity of the later disrupts Purkinje cell firing in *Cacna1a*^{S218L} mutants.

Hyperexcitability of action potential and burst activity by somatic current injections in *Cacna1a*^{S218L} Purkinje cells

To find out the origin of the altered excitability in *Cacna1a*^{S218L} Purkinje cells, we tested the responses to somatic current injections ranging from 100-1000 pA relative to the holding current (see *Experimental Procedures*) (*Fig. 6A, B*). Starting at the lowest current injection tested, *Cacna1a*^{S218L} Purkinje cells fired action potentials, while wild-type

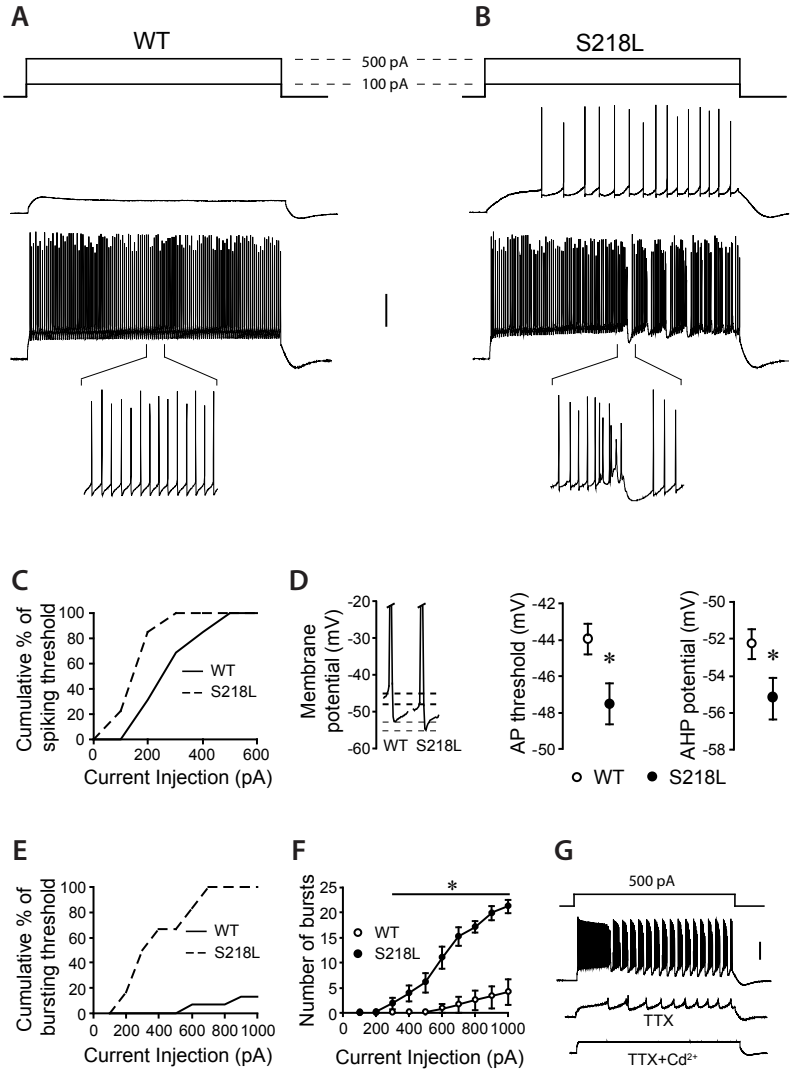

Figure 6. Hyperexcitable action potentials and Ca^{2+}-spikes in *Cacna1a*^{S218L} Purkinje cells. (A, B) Samples of Purkinje cell responses to 1500 ms depolarizing current pulses of 100 and 500 pA in wild-type and *Cacna1a*^{S218L} (Scale bar: vertical 20 mV). Bottom: Purkinje cell responses of short time scale (150 ms) represent regular Na^+ spikes in wild-type and presumed Ca^{2+} spikes in *Cacna1a*^{S218L}. **(C)** Cumulative curve of spiking thresholds plotted against the injected currents in wild-type (n = 13) and *Cacna1a*^{S218L} (n = 13) Purkinje cells. **(D)** (Left panel) Representative examples of action potentials from WT and *Cacna1a*^{S218L} Purkinje cells; (middle panel) mean action potential (AP) threshold and (right panel) after-hyperpolarization (AHP) potentials in wild-type (n = 13) and *Cacna1a*^{S218L} (n = 13) Purkinje cells. **(E)** Cumulative percentage of Purkinje cells firing bursts during the 1500 ms current injections of varying strength. **(F)** Mean number of bursts in response to current injections of 100 - 1000 pA in wild-type (n = 13) and *Cacna1a*^{S218L} (n = 13) Purkinje cells. **(G)** (Top panel) Sample of Purkinje cell responses to 1500 ms long current injections of 500 pA depolarizing current; (middle panel) after application of 1 μM TTX; (bottom panel) and co-application of 1 μM TTX and 100 μM Cd^{2+} (scale bar: vertical 20 mV). Asterisks indicate significant differences (p values indicated in the Results section). See also *Supplementary table 2*.

Purkinje cells remained silent ($p < 0.005$) (*Fig. 6C*). The kinetics of *Cacna1a*^{S218L} Purkinje cell action potentials showed a more hyperpolarized initiation threshold, but otherwise normal kinetics (*Fig. 6D*; *Supplementary table 2*). Increasing the injected current reliably elicited burst-like firing in *Cacna1a*^{S218L} Purkinje cells, whereas such activity was observed only in 2 out of 15 wild-type neurons in response to current injections of ≥ 800 pA ($p < 0.001$) (*Fig. 6E, F*). As previous studies identified similar burst-like activity in Purkinje cells as dendritic Ca^{2+} spikes (*Llinas and Sugimori, 1980*; *Mori et al., 2000*), we repeated the current injection experiment in the presence of the Na^{+}-channel blocker tetrotodoxin (TTX), which abolished the fast somatic action potentials, but not the slow spikes. Co-application of $CdCl_2$, a non-specific Ca^{2+} channel blocker completely abolished the remaining slow spikes, confirming that *Cacna1a*^{S218L} Purkinje cells fire dendritic Ca^{2+} spikes (*Fig. 6G*). Thus, the S218L mutation induces a reduction in the initiation threshold of both action potentials and dendritic Ca^{2+} spikes in *Cacna1a*^{S218L} Purkinje cells.

Cacna1a^{S218L} mutation induces early onset of dendritic burst in a computational Purkinje cell model

To investigate whether the hyperpolarizing shift in Ca^{2+}-channel activation was sufficient to induce the early onset of Ca^{2+} bursting in *Cacna1a*^{S218L} Purkinje cell dendrites, we modeled an isolated piece of Purkinje cell dendrite with active membrane currents that control dendritic excitability to generate Ca^{2+}-spikes. The upstroke and repolarization of the Ca^{2+} spike was facilitated by a high-voltage-activated Ca^{2+} current (CaP) and a Ca^{2+}-activated K^{+} current (KC), respectively, which together realistically modeled the membrane potential responses to current injections (I_{inj}) in wild-type Purkinje cells; low I_{inj} induced a plateau potential and increasing I_{inj} generated Ca^{2+} spikes (*Fig. 7A*). To investigate the effect of the S218L mutation on the excitability of the model, we then shifted the activation of the CaP channel by -12 mV (*Fig. 7B*) to mimic the negative shift in our experimental data (*Fig. 3A*). As a result, the model now only generated plateaus for any value of I_{inj} (*Fig. 7B*). The generation of Ca^{2+} spikes was restored, however, by lowering the CaP channel density to a level comparable to our experimental values and increasing the KC activity (*Fig. 7C, D*). Next, we simulated the combinations of I_{inj} as well as the CaP and KC density that were suitable for eliciting sustained Ca^{2+} spikes in the wild-type (open circles) and *Cacna1a*^{S218L} (solid circles) mice (*Fig. 7D*). The results of these simulations underline that, due to the S218L mutation, less excitatory current is required to facilitate Ca^{2+} spikes. Moreover, in the *Cacna1a*^{S218L} model the Ca^{2+} density required to generate Ca^{2+} spikes significantly increased with higher KC density, which suggests a crucial role for Ca^{2+}-dependent K^{+} (SK) channels in modulating the threshold of Ca^{2+} spikes.

Ca^{2+}-dependent K^{+}-channels modulate dendritic Ca^{2+} spikes in *Cacna1a*^{S218L} Purkinje cells

To test the influence of SK channels on dendritic Ca^{2+} spikes in the *Cacna1a*^{S218L} gain-of-function mutant, we first applied a suboptimal concentration of a SK-channel blocker, since in loss-of-function *Cacna1a* mutants irregular Purkinje cell activity patterns can

be rescued by SK-channel activators (*Walter et al., 2006*). However, bath-application of a potent SK-channel blocker (apamin) did not result in an increase of the threshold (*Fig. 8A*) or a reduction of the number of bursts (*Fig. 8B*) in response to depolarizing somatic current injections to *Cacna1a*^{S218L} Purkinje cells. In fact, apamin increased the occurrence of dendritic Ca^{2+}-spikes. Next, we reasoned that it could also be that the negative shift in $Ca_V2.1$-mediated Ca^{2+} influx in *Cacna1a*^{S218L} Purkinje cells resulted in a lack of Ca^{2+}-dependent K^+-channel function, as suggested by the effects of apamin

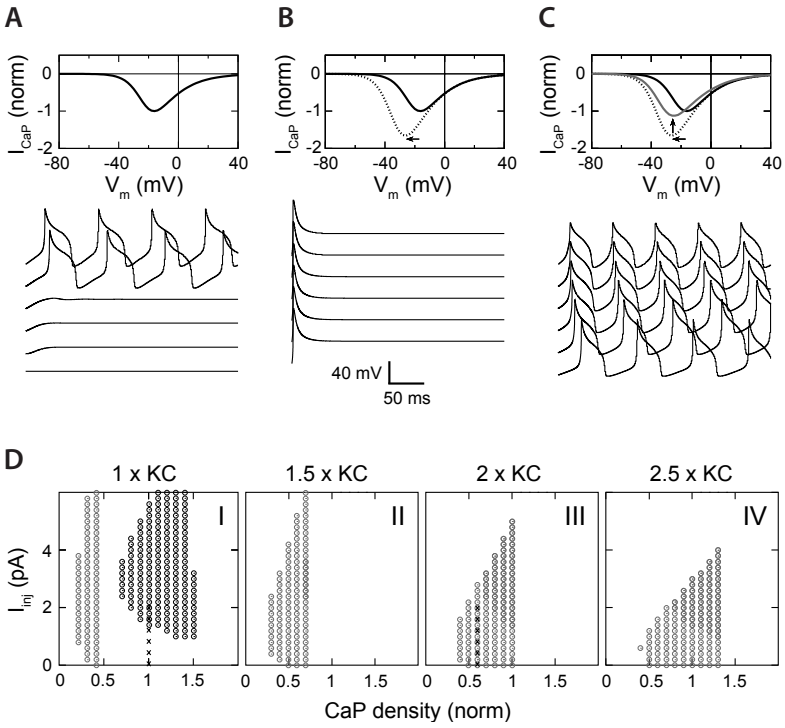

Figure 7. Computational model of early onset of Ca^{2+} bursts in isolated Cacna1a^{S218L} Purkinje cell dendrite. (A) (Top) Simulated Ca^{2+}-current I_{CaP} through a modeled wild-type CaP channel and (bottom) examples of the development of the membrane potential in response to current injections (I_{inj}) increased with 0.4 pA steps. Traces were separated by 40 mV intervals for clarity of display. **(B)** (Top) Shifting the half-maximum activation value $V_{1/2}$ of the CaP channel by 12 mV in the hyperpolarizing direction (as found in *Cacna1a*^{S218L} Purkinje cells; see Fig. 3) and (bottom) the development of the membrane potential with 0.4 pA current injection steps. **(C)** Simulated Ca^{2+}-current I_{CaP} in *Cacna1a*^{S218L} mutant by lowering the Ca^{2+}-current density (grey curve in top panel). Examples of the repetitive Ca^{2+}-spikes with 0.4 pA current injection steps are shown in bottom panel. **(D)** Panel I: Conditions for repetitive calcium spike firing. The dotted areas indicate the combinations of CaP channel density and I_{inj} for which repetitive Ca^{2+}-spiking occurs in the wild-type (black circle) and mutant mice (for which the $V_{1/2}$ of the CaP channel was shifted by 12 mV in the hyperpolarized direction) (gray circle). Panels II, III, and IV indicate the combinations of CaP channel density and I_{inj} conditions for which mutant model display repetitive Ca^{2+} spikes with increasing KC current density. Example curves in (A, B) were taken at the marked locations (crosses) in Panel I. Example curves in (C) were taken at the marked locations in Panel III.

and our computational model (*Fig. 7D*). If correct, a SK-channel activator (1-EBIO; *Pedarzani et al., 2001*) should dampen the bursting activity in *Cacna1a*^{S218L} Purkinje cells. Bath-application of 1-EBIO indeed resulted in a delayed onset of dendritic Ca^{2+} spiking in *Cacna1a*^{S218L} Purkinje cells ($p < 0.03$) (*Fig. 8A*) as well as a reduction of the number of bursts ($p < 0.01$) (*Fig. 8B*), both of which did not differ significantly from wild-type values (both $p > 0.1$). Together these experimental and computational data revealed that the S218L mutation leads to increased dendritic Ca^{2+} spike activity, partially due to a lack of SK-channel function.

DISCUSSION

Although previous studies provide clear evidence how cerebellar ataxia comes about in loss-of-function *Cacna1a* mutants, it remained unclear how gain-of-function mutations in the same gene induce ataxia. We showed that mice harboring the S218L gain-of-function mutation in the *Cacna1a* gene exhibit typical cerebellar hallmarks

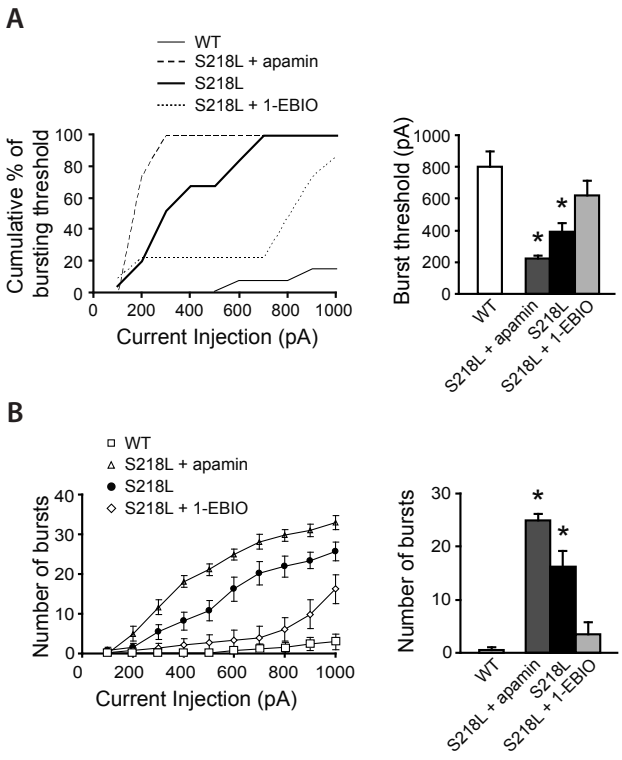

Figure 8. SK channels are involved in controlling Ca^{2+} spike activity. (A) (Left) Cumulative curve of bursting thresholds plotted against the injected currents in *Cacna1a*^{S218L} Purkinje cells with 0.5 nM apamin in the bath (n = 7) and in *Cacna1a*^{S218L} Purkinje cells with 10 µM 1-EBIO in the bath (n = 8). For comparison, the wild-type and *Cacna1a*^{S218L} Purkinje cell data are represented again (as in *Fig. 6*). (Right) Averaged bursting threshold for the four groups represented in left panel. Note that the wild-type values did not differ significantly from the S218L + EBIO group. **(B)** (Left) Similar groups as in (A) but now representing the mean number of bursts in response to 1500 ms current injections of 100-1000 pA. (Right) The average number of bursts at 600 pA of current injection. Note that the application of apamin, SK-channel blocker, increased the bursting activity, whereas 1-EBIO, SK-channel activator, reduced the bursting activity. Asterisks indicate significant differences (p values indicated in the Results section).

of ataxia, such as altered connectivity and transmission at the PF-PC synapse as well as irregular spontaneous Purkinje cell activity. Moreover, our results revealed that the irregular firing of *Cacna1a*^{S218L} Purkinje cells is based upon hyperexcitability; somatic current injections trigger action potentials and dendritic Ca^{2+}-bursts more readily and PF stimulation also results in Ca^{2+}-spikes. Finally, our study revealed that dendritic Ca^{2+} spikes in *Cacna1a*^{S218L} Purkinje cells are enabled by a disbalance between $Ca_V2.1$-mediated Ca^{2+} influx and KC, which is rescued by increasing the SK channel function. Below we will discuss our findings to elucidate their full impact on cerebellar functioning as well as their analogy with those in loss-of-function *Cacna1a* mutants.

Origins of increased synaptic transmission between granule cells and Purkinje cells in *Cacna1a*^{S218L} mice

Our results demonstrate that the S218L gain-of-function *Cacna1a* mutation increases the granule cell input to Purkinje cells by increasing the percentage of PF varicosities that contact multiple Purkinje cell spines and by increasing the synaptic transmission at PF-PC synapses. The increase in connectivity between granule cells and Purkinje cells was counterintuitive, since the same increase in the connectivity was found in various loss-of-function *Cacna1a* mutants and was suggested to be a likely candidate to compensate for the partial loss of synaptic transmission at this synapse (*Rhyu et al., 1999a*; *Rhyu et al., 1999b*; *Miyazaki et al., 2004*). In contrast, the current results indicate that the increased connectivity must be a direct consequence of the offset in Ca^{2+}-homeostasis found in loss- and gain-of-function *Cacna1a* mutants. Although some data describe how this increased connectivity comes about following a complete deletion of the P/Q-type mediated Ca^{2+} currents (*Miyazaki et al., 2004*), it remains to be elucidated how gain-of-function mutations can induce the same morphological aberration. Still, the increased connectivity is likely to amplify the increased synaptic transmission at the PF-PC synapses, especially since our data confirm that the changes in synaptic transmission are due to altered presynaptic Ca^{2+} influx (e.g., the paired-pulse ratio was decreased in *Cacna1a*^{S218L} Purkinje cells, but the kinetics of PF-EPSCs were normal). Thus, the increased Ca^{2+} influx in single PF terminals affects more Purkinje cell spines in *Cacna1a*^{S218L} mutants. Together, these findings indicate that the PF input to *Cacna1a*^{S218L} Purkinje cells is strengthened both structurally and functionally.

In sharp contrast to the differences in PF-PC contacts, we found that the synaptic transmission at the CF-PC synapse is comparatively unaffected in S218L mutants. This was surprising given that a substantial portion of neurotransmitter release from climbing fibers is mediated by $Ca_V2.1$ channels. On the other hand, various loss-of-function *Cacna1a* mutants have been reported to show normal CF-EPSC amplitudes (*Matsushita et al., 2002*; *Liu & Friel, 2008*), which together with our data prove that synaptic transmission at the CF-PC synapse is less vulnerable to Ca^{2+} channelopathies, probably due to the saturated release probability and all-or-none fashion of transmitter release (*Konnerth et al., 1990*; *Matsushita et al., 2002*). Although our results cannot

rule out a possible effect of the decreased τ_{decay} of CF-EPSCs, it seems reasonable to state that the increased PF input to *Cacna1a*^{S218L} Purkinje cells will have a far more dramatic effect on their output, and thereby, on cerebellar functioning. In fact, our results show that modest PF-EPSCs elicit dendritic Ca^{2+} spikes, which, in wild-type, occur predominantly in response to CF stimulation (*Llinas & Sugimori, 1980*).

The *Cacna1a*^{S218L} mutation induces Purkinje cell hyperexcitability and irregular pacemaking activity

The current results show that the S218L mutation causes a negative shift in activation of $Ca_V2.1$ currents in Purkinje cells, which probably leads to irregular pacemaking activity in these cells in two distinct ways. First, *Cacna1a*^{S218L} $Ca_V2.1$ channels are activated at membrane potentials (~-48 mV) that are close to the initiation threshold of Na^+-dependent action potentials (*Llinas & Sugimori, 1980*; *Raman & Bean, 1997*; *Ovsepian & Friel, 2008*). Thus, the lower (e.g., more negative) action potential threshold in *Cacna1a*^{S218L} Purkinje cells could be directly facilitated by the activation of P/Q-type channels. At this point, however, we cannot rule out the possibility that the S218L mutation induces secondary effects on voltage-gated Na^+ and K^+ channels, which may in turn also affect action potential firing in Purkinje cells (see also *Ovsepian & Friel, 2008*). Second, *Cacna1a*^{S218L} Purkinje cells fire dendritic Ca^{2+} spikes upon mild current injections (≥ 200 pA), whereas wild-type Purkinje cells fire such bursts only in response to either climbing fiber activation (*Llinas & Sugimori, 1980*) or strong somatic current injections (≥ 1.0 nA) (*Mori et al., 2000*; *Ovsepian & Friel, 2008*). This finding implies that the negative shift in the activation curve of *Cacna1a*^{S218L} Purkinje cells, possibly together with the decreased branching of proximal Purkinje cell dendrites (*van den Maagdenberg et al., 2010*), promotes backpropagation of depolarizing currents into the dendrites, which has been shown to be poor in wild-type Purkinje cells (*Vetter et al., 2001*). Together, these direct effects of the negative shift in the activation curve are likely to mediate the disturbed intrinsic pacemaking activity in *Cacna1a*^{S218L} Purkinje cells, in that action potential firing in the soma seems to facilitate widespread activation $Ca_V2.1$ channels, which in turn induce burst firing.

In addition to the irregular pacemaking activity in *Cacna1a*^{S218L} Purkinje cells, the negative shift in the $Ca_V2.1$ activation curve also disturbs the Purkinje cell response to PF stimulation. *Cacna1a*^{S218L} Purkinje cells responded with dendritic Ca^{2+}-spikes to modest PF stimuli that only induce normal action potential firing in wild-type Purkinje cells. These Ca^{2+} spikes are presumably enabled by the lower activation threshold of local $Ca_V2.1$ channels, which are densely expressed in the Purkinje cell dendritic tree (*Westenbroek et al., 1995*). This hypothesis is supported by the fact that our computational model of a Purkinje cell dendritic compartment confirmed that Ca^{2+} bursts occur in response to minor current injections as a result of a negative shift in the CaP current. Moreover, when we project the increased PF-EPSC amplitude on the intrinsic hyperexcitability of *Cacna1a*^{S218L} Purkinje cells, it becomes clear that the

PF input further disrupts the irregular pacemaking activity and that all together the firing pattern of *Cacna1a*^{S218L} Purkinje cells is severely disturbed.

Ataxia in gain- and loss-of-function *Cacna1a* mutants

The current study reveals striking similarities between the effects of the *Cacna1a*^{S218L} gain-of-function mutation and those described as consequence of several ataxia-asociated loss-of-function *Cacna1a* mutations. Clearly, PF-PC synapses and Purkinje cells are equally sensitive to increases in $Ca_V2.1$ currents as to their decreases. However, the type of irregular Purkinje cell firing these shifts in $Ca_V2.1$ currents induce differs between S218L gain-of-function mutants and the ataxic loss-of-function mutants. Whereas the hyperexcitability of *Cacna1a*^{S218L} Purkinje cells results in frequent spontaneous or PF-induced burst (e.g., dendritic Ca^{2+} spikes) firing, ataxic *tottering*, *leaner,* and *ducky* mice show a highly irregular pacemaking activity in Purkinje cells, but no spontaneous Ca^{2+} spikes (*Walter et al., 2006*; *Ovsepian & Friel, 2008*). Still, both types of disturbance seem equally detrimental to information processing in the cerebellar cortex and capable of inducing ataxia (*Hoebeek et al., 2005*).

In order to rescue the irregular Purkinje cell firing in loss-of-function mutants SK-channel activators were used previously (*Walter et al., 2006*). Given the accompanying hypothesis that loss-of-function mutants suffered from impaired SK-channel function, we first administered SK-channel blockers to our gain-of-function mutant. The fact that the application of apamin actually worsened the irregularity (e.g., lowered the burst threshold and increased the number of bursts) indicates that the increase in Ca^{2+} influx in S218L mutants might have led to a lack in SK-channel function. This hypothesis was proved by the responses to the SK-channel activator EBIO. Thus, although counterintuitive at first, not only in loss- but also in gain-of-function *Cacna1a* mutants, did the Purkinje cell firing pattern become less irregular after adding SK-channel activators. This suggests that the therapeutical potential of SK-channel activators for treatment of ataxia in *Cacna1a* patients might be wider.

Keeping the irregular *Cacna1a*^{S218L} Purkinje cell firing pattern in mind, we should also consider the potential additional downstream effects of the S218L mutation. For instance, as shown in ataxic loss-of-function mutants, irregular Purkinje cell firing may result in a further loss of information since the propagation reliability of Purkinje cell axons drops at intra-burst frequencies (e.g., > 280 Hz) (*Khaliq & Raman, 2005*; *Monsivais et al., 2005*). Moreover, it is known that (semi-) chronic alterations in Purkinje cell firing patterns can lead to severe morphological aberrations of their axon terminals (*Desclin & Colin, 1980*; *Strata & Montarolo, 1982*; *Rossi et al., 1987*) as was recently described for the loss-of-function *Cacna1a* mutant *tottering* of which cerebellar nuclei neurons indeed show irregular activity patterns (*Hoebeek et al., 2008*). Given that the intrinsic firing pattern of such neurons was recently reported to be regulated predominantly by N-type VGCCs and not affected by blockade of P/Q-type VGCCs (*Alvina & Khodakhah, 2008*), we predict that the firing patterns of *Cacna1a*^{S218L}

cerebellar nuclei neurons are equally disturbed in gain- and in loss-of-function *Cacna1a* mutants.

ACKNOWLEDGEMENTS

We are grateful to E. Haasdijk, E. Goedknegt, M. Rutteman, P. Plak, and Dr. E. Dalm for their technical assistance and to Dr. J.G.G. Borst, E. Galliano, and B. van Beugen for constructive discussions. This work was supported by grants from the Netherlands Organization for Scientific Research (NWO) NWO-ALW (C.I.D.Z. and F.E.H.); NWO-ZON-MW, Neuro-BSIK, EEC-SENSOPAC, and Prinses Beatrix Fonds (C.I.D.Z.); Vici 918.56.602 (M.D.F); and the Center of Medical System Biology (CMSB) established by the Netherlands Genomics Initiative/Netherlands Organisation for Scientific Research (NGI / NWO) and Community (M.D.F. and A.M.J.M.vdM).

SUPPLEMENTARY MATERIAL

Supplementary methods

Stereological quantification. Stereological quantification of Purkinje cell numbers was done on calbindin and Nissl double-stained tissue using an Olympus BH2 Microscope equipped with a motorized stage controlled by computer-run StereoInvestigator 4 software (*MBF Bioscience, Williston, VT*). To estimate the total volume of the cerebellum, virtual contours were drawn around cerebellar tissue. Optical grids (300 × 300 μm^2) including a 3D counting frame (150 × 150 × 15 μm^3) were systematically placed within each contour. Purkinje cells with nucleoli inside the counting frame or contacting the upper and right border of the counting frame were included in the counting, according to standardized criteria (*Gundersen, 1986*). The total Purkinje cell number was estimated using the formula:

$$N = \sum Q \times (t/h) \times (1/asf) \times n$$

where N is the estimation of Purkinje cell number in the cerebellum, ∑Q is the total counted cell number, t is the thickness of the slice, h is the height of the counting frame, asf is the ratio between the area of the frame and the area of the sampling grid, and n is the slice sampling interval. The cerebellar volume was estimated by multiplying the total contour area with the section thickness without correcting for shrinkage factors.

Computational modeling. Mechanisms of dendritic calcium spikes were simulated in a single-compartment model of an isolated piece of Purkinje cell dendrite, using the NEURON environment. The model was used to simulate membrane currents carried by P/Q-type persistent calcium (CaP) channels, a voltage-activated persistent potassium (KM) channels, and two calcium-activated potassium channels (KC and K2), using conventional Hodgkin-Huxley-like formalism with an integration time step of 25 μs. KC, K2 and KM channel descriptions were taken from *De Schutter & Bower* (*1994*) (as implemented in NEURON by *Miyasho et al., 2001*). The CaP channel description was taken from *Khaliq et al.,* (*2003*). The model simulated an isolated piece of Purkinje cell dendrite and consisted of a single cylindrical compartment with length l = 4 μm, diameter d = 2 μm and specific membrane capacitance C_m = 1.64 μF/cm^2. Calcium entering the compartment diffused instantaneously within a thin submembrane shell with thickness d_{shell} = 100 nm. The shell defined a volume that was used to compute the intracellular Ca^{2+}-concentration, which was regulated by Ca^{2+}-entry through membrane channels and removal by a first-order mechanism with rate constant β_{Ca} = 0.6 ms^{-1}. The extracellular Ca^{2+}-concentration was 2 mM, and the internal Ca^{2+}-concentration was not allowed to decrease below 100 nM.

For KC, K2, KM, and leak currents, the current density *i* for was calculated as $i = gm^p h^q z^r (V_m - E)$, where *g* is the conductance density, *m* is an activation variable with *p* order kinetics, *h* is an optional inactivation variable with *q* order kinetics, *z* is an optional Ca^{2+}-dependent activation variable with *r* order kinetics, V_m is the membrane potential and *E* is the reversal potential for the ionic species (E_K = –85mV, E_{Leak} = –80mV). Channel activation and inactivation variables were expressed in terms of a steady state value $m_\infty(V_m)$ and a time constant $\tau_m(V_m)$. Voltage-dependent gating parameters were calculated from a first-order reaction scheme with forward

rate $\alpha(V_m)$ and backward rate $\beta(V_m)$ as $m_\infty = \alpha / (\alpha + \beta)$ and $\tau_m = 1 / (\alpha + \beta)$, except for KM and leak currents, for which they were defined explicitly. Ca^{2+}-dependent gating parameters were calculated as $z_\infty = 1 / (1 + \alpha_Z / [Ca^{2+}])$ and $\tau_Z = \beta_Z$. The specific settings for each current were as follows:

KC: $g = 80$, $p = 1$, $q = 0$, $r = 2$, $\alpha = 7.5$, $\beta = 0.11 / \exp((V_m - 35) / 14.9)$, $\alpha_Z = 40$, $\beta_Z = 10$

K2: $g = 0.39$, $p = 1$, $q = 0$, $r = 2$, $\alpha = 25$, $\beta = 0.075 / \exp((V_m - 5) / 10)$, $\alpha_Z = 0.2$, $\beta_Z = 10$

KM: $g = 0.013$, $m_\infty = 1 / (1 + \exp(-(V_m + 35) / 10))$,
$\tau_m = 3.3(\exp((V_m + 35) / 40) + \exp(-(V_m + 35) / 20)) / 200$

Leak: $g = 0.33$, $m = 1$, $h = 1$, $z = 1$

Conductance densities are in $mScm^{-2}$, voltages in mV.

For the CaP channel, current density was determined as $i_{CaP} = mI_{GHK}$, with m a voltage-dependent gate and I_{GHK} calculated from the Goldman-Hodgkin-Katz current equation. Definitions were as follows:

$$m_\infty = 1 / (1 + \exp(-(V_m + 19) / 5.5))$$

$$\tau_m = \begin{cases} 0.000264 + 0.128\exp(0.103V_m) & V_m \le -35\text{mV} \\ 0.000191 + 0.00376\exp(-((V_m + 41.9) / 27.8)^2) & V_m > -35\text{mV} \end{cases}$$

$$I_{GHK} = 4P_{Ca^{2+}} \frac{VF^2}{RT} \frac{[Ca^{2+}]_i - [Ca^{2+}]_o \exp(-2FV / RT)}{1 - \exp(-2FV / RT)}$$

where $P_{Ca^{2+}} = 1 \times 10^{-2}$ cm/sec, $[Ca^{2+}]_i \ge 100$nM, $[Ca2+]_0 = 2$mM, $T = 310$K, $F = 9.6485 \times 10^4$ C/mol and $R = 8.3145 JK^{-1}mol^{-1}$.

The effects of a mutation in the CaP channel parameters on the initiation of $Ca2^+$ spiking were investigated by introducing a -12 mV offset to the voltage-dependent gate m. The effect of potential compensatory mechanisms in *Cacna1a*^{S218L} Purkinje cell dendrites on persistent Ca^{2+} spiking was investigated by varying the density of CaP and KC currents. Ca^{2+} spikes in the model were detected by implementing a membrane potential threshold criterium, and the occurrence of three or more consecutive threshold crossings was taken as an indication of sustained spiking. The threshold in both models was $V_m = -20$mV.

Supplementary references

1. De Schutter E, Bower JM. An active membrane model of the cerebellar Purkinje cell II. Simulation of synaptic responses. J Neurophysiol. 1994;71:401-19.
2. Gundersen HJ. Stereology of arbitrary particles. A review of unbiased number and size estimators and the presentation of some new ones, in memory of William R. Thompson. J Microsc. 1986;143:3-45.
3. Khaliq ZM, Gouwens NW, Raman IM. The contribution of resurgent sodium current to high-frequency firing in Purkinje neurons: an experimental and modeling study. J Neurosci. 2003;23:4899-912.
4. Miyasho T, Takagi H, Suzuki H, Watanabe S, Inoue M, Kudo Y, Miyakawa H. Low-threshold potassium channels and a low-threshold calcium channel regulate Ca2+ spike firing in the dendrites of cerebellar Purkinje neurons: a modeling study. Brain Res. 2001;891:106-15.

Supplementary figures and tables

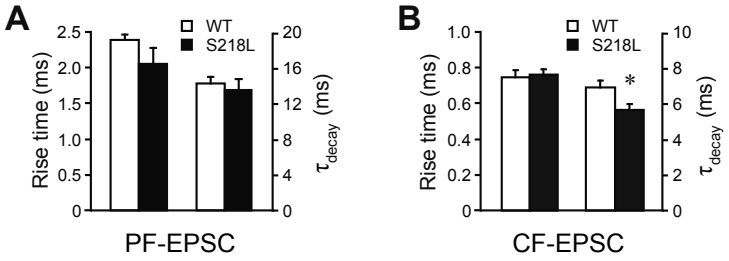

Supplementary figure 1. Kinetics of PF- and CF-EPSCs. (A) Quantification of 10 - 90% rise time (left) and τ_{decay} (right) of PF-EPSCs. **(B)** Quantification of 10 - 90% rise time and τ_{decay} of CF-EPSC. The asterisk indicates significant difference (p values are indicated in the Results section). WT - wild type.

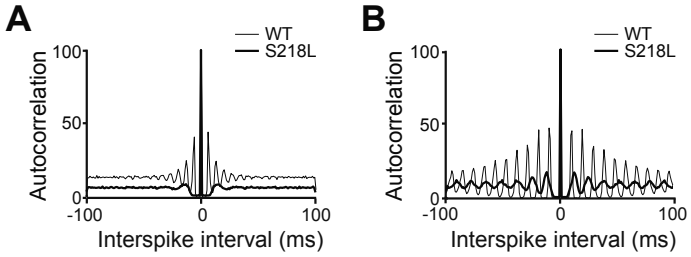

Supplementary figure 2. Autocorrelation of interspike intervals. (A) Representative autocorrelograms of interspike intervals from spontaneous wild-type (thin line) and *Cacna1a*^{S218L} (thick line) Purkinje cell activity. **(B)** as in (A) for intrinsic pacemaking activity.

Supplementary table 1. Quantification of cerebellar volume, Purkinje cell number and dimensions of individual components of PF-PC synapse. Estimated cerebellar volume in mm^3 and total number of Purkinje cells (n = 4 for both wild-type and *Cacna1a*^{S218L}). Quantifications of PF-PC synapses (n = 3 for both wild-type and *Cacna1a*^{S218L}); density of parallel fiber varicosities (PFV) per 20 μm^2 of molecular layer; PFV size; Purkinje cell spine density per 20 μm^2 of molecular layer; Purkinje cell spine length and spine head size; WT - wild-type.

	V_{Cb} (mm^3)	# PC ($\times 10^3$)	PFV density (#/20 μm^2)	PFV size (μm^2)	Spine density (#/20 μm^2)	Spine neck length (μm)	Spine size (μm^2)
WT	35.41 ± 3.01	21.76 ± 5.00	20.27 ± 1.70	0.22 ± 0.02	23.54 ± 1.20	0.99 ± 0.03	0.12 ± 0.01
S218L	36.24 ± 2.10	22.50 ± 5.33	19.30 ± 3.36	0.19 ± 0.03	21.21 ± 0.82	0.98 ± 0.02	0.12 ± 0.01
T-test	0.84	0.42	0.81	0.43	0.21	0.82	0.63

Supplementary table 2. Action potential kinetics. Absolute amplitude of action potential (AP) and after-hyperpolarization (AHP) relative to the AP initiation threshold (see main text for threshold values); half width (HW) (ms) of AP; maximum repolarizing slope (*-dV/dt*) (V/s); and maximum rising slope (*dV/dt*) (V/s) calculated from 19 wild-type and 18 *Cacna1a*^{S218L} Purkinje cells; WT - wild-type.

	AP (mV)	AHP (mV)	HW (ms)	-dV/dt (V/s)	dV/dt (V/s)
WT	69.89 ± 2.18	-7.66 ± 0.40	0.22 ± 0.01	343.32 ± 13.87	397.42 ± 19.66
S218L	66.33 ± 1.64	-6.86 ± 0.59	0.22 ± 0.01	369.00 ± 14.27	399.87 ± 22.07
T-test	0.22	0.27	0.96	0.21	0.93

REFERENCES

1. Alvina K, Khodakhah K. Selective regulation of spontaneous activity of neurons of the deep cerebellar nuclei by N-type calcium channels in juvenile rats. J Physiol. 2008;586:2523-38.
2. Catterall WA, Dib-Hajj S, Meisler MH, Pietrobon D. Inherited neuronal ion channelopathies: new windows on complex neurological diseases. J Neurosci. 2008;28:11768-77.
3. Desclin JC, Colin F. The olivocerebellar system. II. Some ultrastructural correlates of inferior olive destruction in the rat. Brain Res. 1980;187:29-46.
4. Fletcher CF, Lutz CM, O'Sullivan TN, Shaughnessy JD, Jr., Hawkes R, Frankel WN, Copeland NG, Jenkins NA. Absence epilepsy in tottering mutant mice is associated with calcium channel defects. Cell. 1996;87:607-17.
5. Hansel C, de Jeu M, Belmeguenai A, Houtman SH, Buitendijk GH, Andreev D, De Zeeuw CI, Elgersma Y. AlphaCaMKII Is essential for cerebellar LTD and motor learning. Neuron. 2006;51:835-43.
6. Hoebeek FE, Khosrovani S, Witter L, De Zeeuw CI. Purkinje cell input to cerebellar nuclei in tottering: ultrastructure and physiology. Cerebellum. 2008;7:547-58.
7. Hoebeek FE, Stahl JS, van Alphen AM, Schonewille M, Luo C, Rutteman M, van den Maagdenberg AM, Molenaar PC, Goossens HH, Frens MA, De Zeeuw CI. Increased noise level of purkinje cell activities minimizes impact of their modulation during sensorimotor control. Neuron. 2005;45:953-65.
8. Holt GR, Softky WR, Koch C, Douglas RJ. Comparison of discharge variability in vitro and in vivo in cat visual cortex neurons. J Neurophysiol. 1996;75:1806-14.
9. Imbrici P, Eunson LH, Graves TD, Bhatia KP, Wadia NH, Kullmann DM, Hanna MG. Late-onset episodic ataxia type 2 due to an in-frame insertion in CACNA1A. Neurology. 2005;65:944-6.
10. Jorntell H, Ekerot CF. Properties of somatosensory synaptic integration in cerebellar granule cells in vivo. J Neurosci. 2006;26:11786-97.
11. Khaliq ZM, Raman IM. Axonal propagation of simple and complex spikes in cerebellar Purkinje neurons. J Neurosci. 2005;25:454-63.
12. Konnerth A, Llano I, Armstrong CM. Synaptic currents in cerebellar Purkinje cells. Proc Natl Acad Sci USA. 1999;87:2662-5.
13. Kors EE, Terwindt GM, Vermeulen FL, Fitzsimons RB, Jardine PE, Heywood P, Love S, van den Maagdenberg AM, Haan J, Frants RR, Ferrari MD. Delayed cerebral edema and fatal coma after minor head trauma: role of the CACNA1A calcium channel subunit gene and relationship with familial hemiplegic migraine. Ann Neurol. 2001;49:753-60.
14. Kulik A, Nakadate K, Hagiwara A, Fukazawa Y, Lujan R, Saito H, Suzuki N, Futatsugi A, Mikoshiba K, Frotscher M, Shigemoto R. Immunocytochemical localization of the alpha 1A subunit of the P/Q-type calcium channel in the rat cerebellum. Eur J Neurosci. 2004;19:2169-78.
15. Liu S, Friel DD. Impact of the leaner P/Q-type Ca2+ channel mutation on excitatory synaptic transmission in cerebellar Purkinje cells. J

Physiol. 2008;586:4501-15.

16. Llano I, Marty A, Armstrong CM, Konnerth A. Synaptic- and agonist-induced excitatory currents of Purkinje cells in rat cerebellar slices. J Physiol. 1991;434:183-213.
17. Llinas R, Sugimori M. Electrophysiological properties of in vitro Purkinje cell somata in mammalian cerebellar slices. J Physiol. 1980;305:171-95.
18. Matsushita K, Wakamori M, Rhyu IJ, Arii T, Oda S, Mori Y, Imoto K. Bidirectional alterations in cerebellar synaptic transmission of tottering and rolling Ca2+ channel mutant mice. J Neurosci. 2002;22:4388-98.
19. Mintz IM, Venema VJ, Swiderek KM, Lee TD, Bean BP, Adams ME. P-type calcium channels blocked by the spider toxin omega-Aga-IVA. Nature. 1992;355:827-9.
20. Miyazaki T, Hashimoto K, Shin HS, Kano M, Watanabe M. P/Q-type Ca2+ channel alpha1A regulates synaptic competition on developing cerebellar Purkinje cells. J Neurosci. 2004;24:1734-43.
21. Monsivais P, Clark BA, Roth A, Hausser M. Determinants of action potential propagation in cerebellar Purkinje cell axons. J Neurosci. 2005;25:464-72.
22. Mori Y, Wakamori M, Oda S, Fletcher CF, Sekiguchi N, Mori E, Copeland NG, Jenkins NA, Matsushita K, Matsuyama Z, Imoto K. Reduced voltage sensitivity of activation of P/Q-type Ca2+ channels is associated with the ataxic mouse mutation rolling Nagoya (tg(rol)). J Neurosci. 2000;20:5654-62.
23. Ophoff RA, Terwindt GM, Vergouwe MN, van Eijk R, Oefner PJ, Hoffman SM, Lamerdin JE, Mohrenweiser HW, Bulman DE, Ferrari M, Haan J, Lindhout D, van Ommen GJ, Hofker MH, Ferrari MD, Frants RR. Familial hemiplegic migraine and episodic ataxia type-2 are caused by mutations in the Ca2+ channel gene CACNL1A4. Cell. 1996;87:543-52.
24. Ovsepian SV, Friel DD. The leaner P/Q-type calcium channel mutation renders cerebellar Purkinje neurons hyper-excitable and eliminates Ca2+-Na+ spike bursts. Eur J Neurosci. 2008;27:93-103.
25. Pedarzani P, Mosbacher J, Rivard A, Cingolani LA, Oliver D, Stocker M, Adelman JP, Fakler B. Control of electrical activity in central neurons by modulating the gating of small conductance Ca2+-activated K+ channels. J Biol Chem. 2001;276:9762-9.
26. Raman IM, Bean BP. Resurgent sodium current and action potential formation in dissociated cerebellar Purkinje neurons. J Neurosci. 1997;17:4517-26.
27. Regehr WG, Mintz IM. Participation of multiple calcium channel types in transmission at single climbing fiber to Purkinje cell synapses. Neuron. 1994;12:605-13.
28. Rhyu IJ, Abbott LC, Walker DB, Sotelo C. An ultrastructural study of granule cell/Purkinje cell synapses in tottering (tg/tg), leaner (tg(la)/tg(la)) and compound heterozygous tottering/leaner (tg/tg(la)) mice. Neuroscience. 1999;90:717-28.
29. Rhyu IJ, Oda S, Uhm CS, Kim H, Suh YS, Abbott LC. Morphologic investigation of rolling mouse Nagoya (tg(rol)/tg(rol)) cerebellar Purkinje cells: an ataxic mutant, revisited. Neurosci Lett. 1999;266:49-52.
30. Rossi F, Cantino D, Strata P. Morphology of Purkinje cell axon terminals in intracerebellar nuclei following inferior olive lesion. Neuroscience. 1987;22:99-112.
31. Strata P, Montarolo PG. Functional aspects of the inferior olive. Arch Ital Biol. 1982;120:321-9.
32. Tottene A, Pivotto F, Fellin T, Cesetti T, van den Maagdenberg AM, Pietrobon D. Specific kinetic alterations of human CaV2.1 calcium channels produced by mutation S218L causing familial hemiplegic migraine and delayed cerebral edema and coma after minor head trauma. J Biol Chem. 2005;280:17678-86.
33. Vahedi K, Joutel A, Van Bogaert P, Ducros A, Maciazeck J, Bach JF, Bousser MG, Tournier-Lasserve E. A gene for hereditary paroxysmal cerebellar ataxia maps to chromosome 19p. Ann Neurol. 1995;37:289-93.
34. van den Maagdenberg AM, Pietrobon D, Pizzorusso T, Kaja S, Broos LA, Cesetti T, van de Ven RC, Tottene A, van der Kaa J, Plomp JJ, Frants RR, Ferrari MD. A Cacna1a knockin migraine mouse model with increased susceptibility to cortical spreading depression. Neuron. 2004;41:701-10.
35. van den Maagdenberg AM, Pizzorusso T, Kaja S, Terpolilli N, Shapovalova M, Hoebeek FE, Barrett CF, Gherardini L, van de Ven R, Todorov B, Broos L, Tottene A, Gao Z, Fodor M, De Zeeuw CI, Frants RR, Plesnila N, Plomp JJ, Pietrobon D, Ferrari MD CaV2.1 S218L knockin mice exhibit the severe human S218L migraine syndrome of episodic hemiplegia, epilepsy, cerebral edema, and ataxia, and are uniquely vulnerable to cortical spreading depression. Ann Neurol. 2010;67:85-98.
36. Vetter P, Roth A, Hausser M. Propagation

of action potentials in dendrites depends on dendritic morphology. J Neurophysiol. 2001;85:926-37.

37. von Brederlow B, Hahn AF, Koopman WJ, Ebers GC, Bulman DE. Mapping the gene for acetazolamide responsive hereditary paryoxysmal cerebellar ataxia to chromosome 19p. Hum Mol Genet. 1995;4:279-84.
38. Wakamori M, Yamazaki K, Matsunodaira H, Teramoto T, Tanaka I, Niidome T, Sawada K, Nishizawa Y, Sekiguchi N, Mori E, Mori Y, Imoto K. Single tottering mutations responsible for the neuropathic phenotype of the P-type calcium channel. J Biol Chem. 1998;273:34857-67.
39. Walter JT, Alvina K, Womack MD, Chevez C, Khodakhah K. Decreases in the precision of Purkinje cell pacemaking cause cerebellar dysfunction and ataxia. Nat Neurosci. 2006;9:389-97.
40. Westenbroek RE, Sakurai T, Elliott EM, Hell JW, Starr TV, Snutch TP, Catterall WA. Immunochemical identification and subcellular distribution of the alpha 1A subunits of brain calcium channels. J Neurosci. 1995;15:6403-18.
41. Zhuchenko O, Bailey J, Bonnen P, Ashizawa T, Stockton DW, Amos C, Dobyns WB, Subramony SH, Zoghbi HY, Lee CC. Autosomal dominant cerebellar ataxia (SCA6) associated with small polyglutamine expansions in the alpha 1A-voltage-dependent calcium channel. Nat Genet. 1997;15:62-9.